Pre-Vaporized Ignition Behavior of Ethyl- and Propyl-Terminated Oxymethylene Ethers

Stephen P. Lucas[a], Nicole J. Labbe[b], Anthony J. Marchese[c], Bret Windom[a,*]

[a] *Department of Mechanical Engineering, Colorado State University, 400 Isotope Drive, Fort Collins CO 80521 United States of America*
[b] *Paul M. Rady Department of Mechanical Engineering, University of Colorado Boulder, 1111 Engineering Drive Boulder CO 80309, United States of America*
[c] *College of Engineering, University of Rhode Island, Kingston, RI, 02881, United States of America*

23 August 2022

Abstract

Oxymethylene ethers (OMEs) have been studied in recent years for use as compression ignition fuel blendstocks, but the methyl-terminated OMEs commonly studied exhibit properties that are poorly optimized for engine use and distribution. Recent work has shown that OMEs with larger (ethyl, propyl, or butyl) end groups may have superior properties for fuel usage/storage. In this work, we consider ignition of four OMEs - diethoxymethane (E-1-E), dipropoxymethane (P-1-P), ethoxy-(methoxy)$_2$-ethane (E-2-E), and diisopropoxymethane (iP-1-iP) - as representatives of the possible effects of changes to OME structures. To our knowledge, ignition behaviors of the latter three fuels have not been studied prior to this work. We find that all of the tested linear OMEs (E-1-E, P-1-P, and E-2-E) show two-stage ignition at low temperatures and nonlinear ignition behavior, consistent with literature on methyl-terminated OMEs and E-1-E. The nonlinear, branched OME (iP-1-iP) required higher pressure and temperature to ignite than the linear OMEs; further, this fuel experienced only single stage ignition and a linear ignition delay curve. By analogy to existing kinetic mechanisms for ethers and higher alcohols, the chemical basis for the observed trends are hypothesized. Faster ignition of E-2-E results from the additional oxymethylene group providing additional sites for ROO formation and more possible QOOH structures. Slower low temperature ignition of P-1-P is driven by lower H abstraction rates in comparison to E-1-E, however at high temperatures P-1-P ignites faster, driven by increasing abstraction from the additional H site on the propyl group that opens up additional QOOH formation pathways. iP-1-iP ignition is slowed significantly by preferential H abstraction from the central carbon of the isopropyl group, which is crowded and unlikely to bond with O_2, however at high temperatures, abstraction from H sites on the methyl groups allows for the ROO cascade initiation and subsequent rapid ignition.

Keywords: Oxymethylene ether; Rapid compression machine; Oxygenated fuels; Low emission fuels; Fuel reactivity

* Corresponding Author. *Email:* Bret.Windom@colostate.edu (B. Windom).

1. Introduction

In recent years, there has been a global effort to improve the operation of internal combustion engines in order to increase efficiency and reduce emissions. Multiple jurisdictions have implemented programs targeting improvements in fuel and engine technology to achieve these goals, such as the European Union under the Transport Research and Innovation Monitoring and Information System, and the United States under the Department of Energy Co-Optimization of Fuels & Engines initiative. Efforts to combat climate change factor strongly into these initiatives, as well as possible cost reductions from improved efficiency, and health benefits from reduced emissions.

A promising alternative fuel type that has been investigated for use in compression ignition (CI) engines is the class of molecules known as oxymethylene ethers (OMEs). These molecules comprise of at least one oxymethylene (-CH_2O-) unit bonded to an additional oxygen and terminating alkyl groups; dimethoxymethane is the simplest OME with only one oxymethylene unit terminated by two methyl end groups. More recently, larger methyl-terminated OMEs with 3-7 oxymethylene units (also referred to as polyoxymethylene dimethyl ethers) have garnered significant interest for use as a diesel fuel blendstock as they have potential to be renewably sourced either from biomass feedstocks or via electrofuel production pathways while exhibiting favorable combustion properties including high cetane numbers and very low sooting propensity [1–4].

While methyl terminated OMEs exhibit extraordinary promise with regards to their combustion, concerns with their low energy density [5], high water solubility [6], and poor seal material compatibility [3, 7], are likely to prevent wide spread adoption. Most research has focused on methyl-terminated OMEs, with some works also considering ethyl-terminated ethers [5, 8–11], however, recently, Bartholet et al. [6] published a predictive modeling approach which explored a large range of possible OME molecules and demonstrated that the optimal OME structures for use in CI engines, when accounting for not only combustion behaviors but also properties important for fuel handling and storage, may be those with higher terminating alkyl groups (e.g., ethyl, propyl, and butyl groups) and moderate length (1-3) oxymethylene chains.

In this work, we test several candidate OMEs with larger (C_2 and C_3) alkyl end groups in a rapid compression machine (RCM) to determine their ignition characteristics, and observe the effects of changing various aspects of the molecular structure, namely, extending the alkyl length, extending the oxymethylene chain, and the use of linear vs branched end group structures, on their ignition behavior. As there are no existing chemical mechanisms for several of the tested molecules, analogies are drawn to the reaction chemistry of well-understood molecules such as simple ethers, methyl-terminated OMEs, and higher alcohols to explain the observed behaviors of the various OMEs. Several prior works [8–11] have considered the ignition behaviors and chemical kinetics of one of our candidates (diethoxymethane), and we draw upon this literature to compare with and ensure consistency, but to our knowledge, there has not been any published research into the ignition behavior of the other tested OME fuels.

2. Methods

2.1. Candidate Fuels & Chemical Preparation

Four OMEs were selected for this analysis, each representing a unique modification in the structure of the OME. For simplicity, we abbreviate each fuel, X-n-Y, representing the first alkyl end group, *X*, the number of oxymethylene units, *n*, and the second alkyl group, *Y*. The structures for these molecules are presented in Fig. 1. Here we label each of the carbons for ease of discussion, starting with the end group carbon closest to the ether oxygen labeled as α, and so forth. For all OMEs presented, all carbons between the ether moieties are labeled δ for consistency.

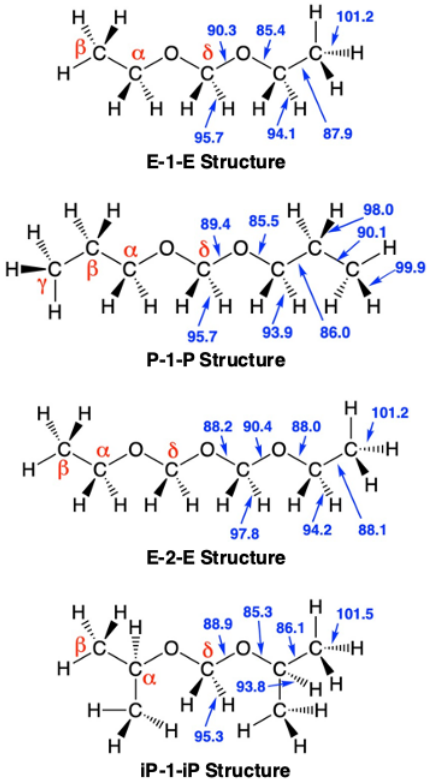

Fig. 1: OME Structures: Red greek letter indicate carbon labels. Blue numbers indicate bond dissociation energies in kcal/mol from [12–14]

The simplest OME tested in this study is diethoxymethane (3,5-dioxaheptane, referred to here as

Table 1: Relevant properties of sample and reference fuels. n-C7, i-C8 data from [15][a] , [16][b]

Fuel	ICN	Boiling Point [°C]	Flash Point [°C]	LHV [MJ/kg]
E-1-E	41.1	88	<20	28.8
E-2-E	60.3	142	35.5	25.9
P-1-P	53.2	141	31.7	32.0
iP-1-iP	11.2	119	21.3	31.4
n-C_7	57.6[a]	99[b]	<20[b]	44.9[b]
i-C_8	5.2[a]	114[b]	<20[b]	44.7[b]
Diesel	>40	n/a	>52	>42

E-1-E), the ignition and kinetics of which have been previously studied, providing a basis for comparison to our results [8, 9, 11, 17]. Dipropoxymethane (4,6-dioxanonane, here P-1-P) has been characterized for fuel properties by Drexler et al. [18], but has not, to our knowledge, been tested for ignition behaviors. We use this fuel to consider the effects of lengthening the alkyl terminations. Ethoxy-(methoxy)$_2$-ethane (3,5,7-trioxanonane, here E-2-E) has been studied prior by Lautenschutz [5], but no kinetics or ignition delay experiments have been performed. Finally, diisopropoxymethane (2,2'-[methylenebis(oxy)]bis-propane, here iP-1-iP) is a new, unstudied molecule, representing a change from a linear OME structure analogous to normal alkanes, to a branched OME structure analogous to isoalkanes. Each of these molecules have similar bond dissociation energies (BDEs) for equivalent bonds as shown in units of kcal/mol in Fig. 1. All BDE values were obtained using the ALFABET tool from the National Renewable Energy Laboratory (NREL) [12–14]. When available, density functional theory values were preferred over machine learning values.

E-1-E was purchased from Sigma-Aldrich at >99% purity. P-1-P was provided as a sample from Lambiotte & Cie at 97.5% purity (balance P-2-P). E-2-E and iP-1-iP are not commerically available and were synthesized. Synthesis of extended oxymethylene ethers is a well-developed process, reviewed in detail in works such as [19]. The most common method of producing extended oxymethylene ethers is through the reaction of n=1 OMEs with trioxane over acid catalyst; for this work we reacted E-1-E with trioxane over Amberlyst 15 to produce a mixture of E-1-E, E-2-E, and higher oligomers. After reaction, the mixture was washed with a sodium carbonate and sodium bicarbonate buffer solution (pH = 9) to remove remaining trioxane and paraformaldehydes, and then distilled in a BR Instruments spinning-band vacuum distillation column to 95.3% purity, balance 1.6% E-1-E and 3.1% E-3-E.

Synthesis of extended-alkyl oxymethylene ethers can be performed in multiple ways; the simplest method in literature is the trans-acetalization reaction of methyl-terminated OMEs with higher alcohols [20], which also produces asymmetric OMEs with two different end group types. It has been demonstrated that dimethoxymethane can be synthesized from methanol and a formaldehyde source [21]; we apply this same method to higher alcohols to produce novel OMEs. Having verified that this method reliably produces diethoxymethane, dipropoxymethane, and dibutoxymethane by comparison of distilled products with commercially available samples, we react isopropanol with trioxane in 6:1 ratio (2:1 ratio to formaldehyde) to produce the iP-1-iP sample (the same buffer solution and distillation process described earlier is used to wash and purify) with purity 97.5%, balance 2% iP-2-iP and 0.5% trioxane. Due to the hydrophilic nature of oxygenated compounds, samples for RCM use were stored over 4A molecular sieves to prevent uptake of atmospheric water vapor.

Physicochemical properties relevant for diesel fuel were measured or extracted from the literature for the tested OMEs and are provided in Table 1. These and addtional fuel properties for a wide range of OMEs are documented in [22]. Indicated Cetane Numbers (ICN) were measured using a constant volume combustion chamber (the details of which are provided in [15, 23]) following ASTM D8183 [24]. Flash Points were measured per ASTM D93A [25], and the lower heating value (LHV) was measured in an IKA C200 calorimeter. Values for n-heptane (n-C_7) and iso-octane (i-C_8) along with minimum diesel fuel specifications are also provided in Table 1 for reference. While the linear OMEs have ICNs close to or exceeding diesel fuel requirements, similar to n-heptane, iP-1-iP has a very low cetane number, more comparable to iso-octane [15] and perhaps better suited for gasoline than diesel blending.

2.2. Rapid Compression Machine System Description

The RCM used in this work is a dual piston, hydraulically locked, pneumatically driven machine. The pistons used are creviced to capture roll-up vortices and improve the uniformity of the compressed gas core [26, 27]. Monitored low speed variables include pressure and temperature in a heated mixing tank, temperature of the heat-traced fill line, chamber fill pressure, and temperature of the piston sleeves, which we assume to be equivalent to uncompressed gas temperature. High-speed data were recorded for chamber pressure (Kistler 601CAA with Kistler Type 2018 charge amplifier) and piston position (2x Positek P100.230GL100NSUZ465). A schematic of the system is provided in supplementary material Fig. S1; a more detailed description of the machine systems may be found in Boissiere [28].

All fuels were tested in a dilute environment (12 mol inert gas : 1 mol O_2), as has been done in prior work with OMEs for ignition delay time (IDT) [9, 11], with a stoichiometric fuel/O_2 ratio. To allow for the range of desired temperatures, multiple inert gas mixtures were used with varying ratios of CO_2, N_2, and Ar. A summary of conditions used is provided in Table 2; supplementary Table S1 includes

Table 2: Description of test conditions used in RCM. Effective CR is compression ratio required to achieve observed TDC pressure if compression was isentropic. See Table S1 for exact data from each test point.

Inert Composition	Typical Temp Range [K]	Typical Eff. CR
0.5 CO_2, 0.5 N_2	675-715	10.5
0.25 CO_2, 0.75 N_2	690-755	10.4
N_2	730-840	10.7
0.8 N_2, 0.2 Ar	830-930	10.3
0.6 N_2, 0.4 Ar	910-1010	9.8
0.4 N_2, 0.6 Ar	990-1110	9.3

composition data for each test point. DOIs for accessing the full test dataset are provided in Table S2. The gas mixtures were created barometrically at 60 °C in a separate, heated and stirred mixing tank (fuels were added first, volumetrically, as liquids prior to gas addition), and no tests were run sooner than 1 hour after forming the mixture to allow for the gases to become uniformly mixed. Accelerated autooxidation testing indicated acceptable stability of these molecules [22] and no reactions are expected in the mixing tank.

2.3. Analysis Algorithm Methodology

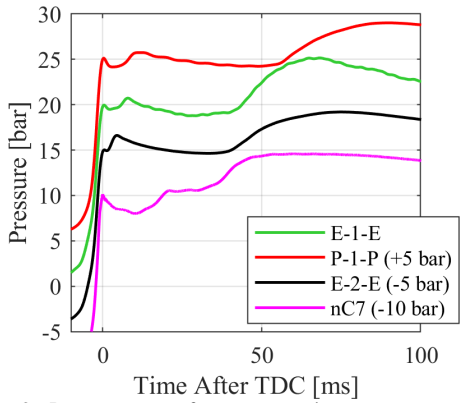

Fig. 2: Pressure traces for representative tests at approximately 700K and 20 bar.

In this work, the IDT was defined as the intersection of tangents of maximum gradient and of the local minimum pressure prior to the pressure rise due to reaction; this method is essentially equivalent to that described in [29] but applied to the dynamic pressure here rather than [OH*]. We note that this is different from common methods for RCMs; as reviewed by Zhang et al. [30], RCM IDT is often defined as either the root of the tangent line at the inflection point of pressure rise, or the inflection point itself. This alternative method is used due to the low dP/dt of these fuels at lower temperatures, where the first of the common methods would significantly underpredict, and the second would overpredict, the time when reactions begin to rapidly branch. Tests were performed with n-heptane confirming that these low heat release rates were not unique behaviors of OMEs; sample pressure traces shown in Fig. 2 indicate that n-heptane experiences similar slow pressure rise at the low temperature and dilute conditions. At higher temperatures and higher dP/dt, there is little difference between the two common methods and our approach here, while at lower temperatures we may observe differences of approximately 5-8 ms. An example of this method is shown in Fig. S2.

As the compressed temperature at TDC is calculated from the pressure trace, assuming an isentropic core [27], the method of filtering the pressure trace can affect peak (TDC) temperature and pressure. We find the variance to be approximately +/-5 K and +/-0.1 bar within the range of frequencies that produce an accurate, low-noise pressure curve from a low-pass filter. The compression stroke produced the target pressure to an average of 20.1 bar with 1.55% (0.311 bar) standard deviation. Transient temperatures are calculated using the change in pressure, assuming isentropic compression at each time step (Δt = $5\text{x}10^{-7}$s), with the specific heat ratio (γ) of the oxygen and inert gases calculated using polynomials from the Lawrence Livermore n-heptane mechanism [31]. For the fuels, specific heat for E-1-E was calculated from the polynomials used in Li et al. [11]; the other OMEs do not have published thermodynamic data, so specific heat polynomials were calculated from the MIT Reaction Mechanism Generator (RMG), which uses group additivity methods [32]. The RMG calculation was compared with results from Li for E-1-E and was within 5% for 600K-1000K, indicating acceptable accuracy of these methods for this work. Initial temperatures were measured via a thermocouple to an accuracy of +/- 1 K, which transforms to +/- 3.55 K at TDC temperature for an average effective compression ratio of 10 (see Table S1 for these values) in a 40% N_2 / 60% Ar bath gas environment (the highest γ gas mixture used). Combining errors, the pressure is accurate to +/- 0.327 bar, and the temperature to +/- 6.13 K. Using sample E-1-E pressure traces at 720 K and 915 K (experiencing two stage and single stage ignition, respectively), testing the range of reasonable filtering techniques provided a range of +/-7% for first stage IDT and +/-5% for primary IDT. Temperature errors of +/-6.13 K at 720 K and 915 K produce IDT errors of +/-6% and +/-1%, respectively. Combining these errors, we expect an accuracy of +/-11% for IDT measurements.

3. Results

The observed ignition behavior of the OMEs generally fell into three categories: at lower temperatures, the linear OMEs (E-1-E, E-2-E, and P-1-P) demonstrated multi-stage ignition with relatively low pressure gradients (see Fig. 2). As the temperature increased, the first stage ignition disappeared, resulting in single stage ignition with a faster rate of pressure

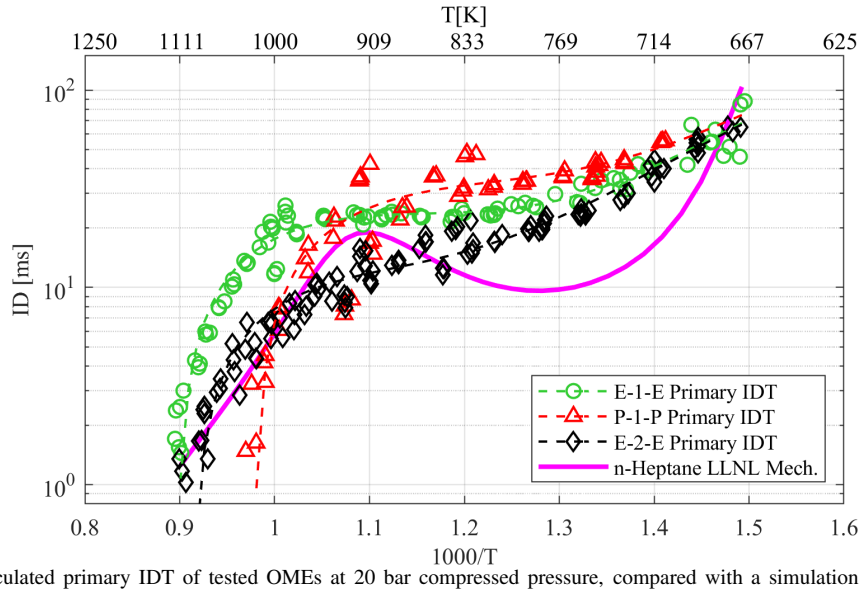

Fig. 3: Calculated primary IDT of tested OMEs at 20 bar compressed pressure, compared with a simulation of n-heptane (Lawrence Livermore National Lab n-Heptane Detailed Mechanism Version 3 [31]) at comparable conditions.

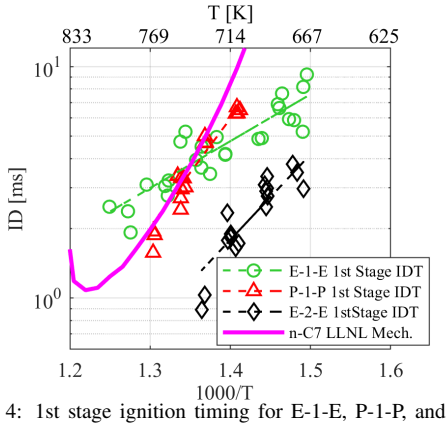

Fig. 4: 1st stage ignition timing for E-1-E, P-1-P, and E-2-E, when observed, compared with a simulation of n-heptane (Lawrence Livermore National Lab n-Heptane Detailed Mechanism Version 3 [31]) at comparable conditions.

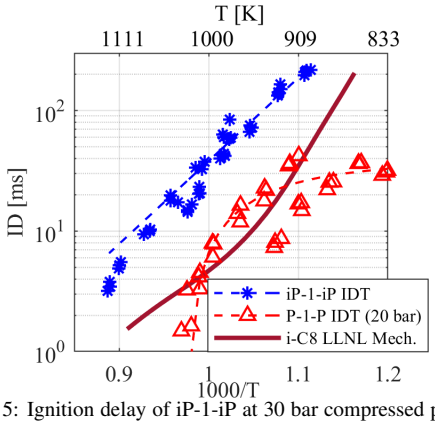

Fig. 5: Ignition delay of iP-1-iP at 30 bar compressed pressure, compared with simulation of iso-octane at comparable conditions (Lawrence Livermore National Lab Iso-Octane Version 3 [33]), and P-1-P at 20 bar.

rise. Finally, the branched OME (iP-1-iP) only ever demonstrated single stage ignition; further, this fuel was incapable of ignition at the 20 bar compressed pressure used in earlier tests. At 30 bar, high temperatures were required to initiate ignition and the IDT fell rapidly with increasing temperature afterward.

The primary IDT for all of the tests at 20 bar where ignition occurred (tests at temperatures too low for ignition were performed, but are not shown here) is shown in Fig. 3. First stage IDT, when observed, are shown in Fig. 4. Trend lines are provided for each data set as dotted lines; a third-order polynomial describes the linear OME behavior to $R^2 > 0.90$. iP-1-iP ignition required higher pressure (30 bar) and its IDTs are shown in Fig. 5 alongside those of P-1-P at 20 bar for comparison; iP-1-iP behavior is linear on this chart (exponential fit $R^2 = 0.98$). In Figs. 3 and 4, the calculated IDT of n-heptane [31] using Chemkin simulation provides a reference to a more well-studied fuel; similarly, Fig. 5 includes calculated iso-octane IDT [33]. We consider the chemical basis of observed behavior later in this section; however, on a broad scale there are some basic observations. First, we observe that all of the tested linear OMEs show strong nonlinear temperature dependencies, but not true negative temperature coefficient behavior as seen with n-heptane. Secondly, iP-1-iP behaves similar to iso-octane without apparent nonlinearity, but has delayed ignition.

Prior literature, e.g. [26], notes that discontinuities

in IDT curves may occur with changes in diluent gas composition, particularly with increasing argon concentration, where ignition slows for a given temperature condition due to thermal effects. We note some of this behavior in our data, most apparently for the P-1-P at just above 1000/T = 1.1; for E-1-E and E-2-E these effects are observable but less apparent as they occur in a region where the IDT is nearly unaffected by the temperature and thus thermal effects will produce less noticeable changes in IDT. Prior literature studying fuels with established chemical mechanisms, e.g. [34, 35], have noted that at higher temperatures and shorter IDTs, the effects on IDT of radical formation during the compression stroke may not be negligible. Consequently, we caution the reader that the reported high-temperature IDT may be shorter than would occur if TDC conditions were achieved instantaneously without facility effects, and simulations of these conditions should include the compression stroke.

As a primary point of comparison, we will first consider the behavior of E-1-E, as its ignition has been characterized; we direct the reader to [8, 10, 11] for detailed discussion of the kinetics of this fuel. Here, E-1-E shows a wide region (750 - 1000 K) where IDT is essentially independent of temperature. Lehrheuer et al. [9] observed similar behavior in prior RCM testing of this fuel at these dilute conditions (we note that their observed IDT is faster as their tests were performed at 30 bar compressed pressure); similarly, kinetic modeling by Li et al. [11] shows a small temperature-independent region, although their modeling is primarily performed with standard air (3.76:1 inert to oxygen ratio).

3.1. Effect of Extending the Oxymethylene Chain

Using E-1-E as a reference, it can be observed that adding an additional oxymethylene unit (E-1-E $\longrightarrow$ E-2-E) advances the ignition at moderate to high temperatures (although it is worth noting that at low temperatures, $<$750 K, E-1-E and E-2-E have comparable IDT), and advances the temperature where IDT begins to rapidly decrease. This behavior is similar to that observed by Cai et al. [36] when transitioning between methyl-terminated OMEs of various oxymethylene chain lengths, although one can note from the above work that this reduction appears to have a diminishing effect as the chain length continues to increase, with the largest change occurring with an increase from one to two oxymethylene units. Additionally, as shown in Fig. 2, at low temperatures, the first stage ignition of E-2-E is faster by a few milliseconds - not a large change in comparison to the primary IDT, but roughly twice as fast as E-1-E for the first stage only. A test of n-heptane at comparable conditions shows that the n=1 OMEs have similar first stage ignition timing to n-heptane, while the all of the OMEs have slower primary ignition at these low-temperature conditions.

In their analysis of diethoxymethane decomposition, Jacobs et al. [10] found that as temperature was increased, the diethoxymethane radical formed after H-abstraction from the central methylene group (analogous to the δ-E-1-E radical) and rapidly β-scissioned to form ethyl formate rather than react bimolecularly with O_2 to form a peroxyl radical, essentially inhibiting hydroxyl formation and retarding ignition. Notably, the reaction rates for the decomposition of δ-E-1-E used in their model were the highest pressure rates from Kroger et al. [8] and may be too fast by as much as a factor of 20 for the 10 bar IDT experimental conditions, potentially exaggerating the observation. Li et al. [11] similarly noted the importance of the δ-E-1-E radical on inhibiting ignition at higher temperatures, though they attributed the effect to the lesser number of unique peroxyl radicals that can be formed as compared to the other diethoxymethane radicals. Similar arguments may be made to explain the faster reactivity of E-2-E. Fig. 1 shows that the C-O bond attached to α-carbon is slightly stronger for E-2-E (2.6 kcal/mol), which would slow β-scission of the δ-E-2-E radical and provide more opportunity for ROO formation. Furthermore, the symmetry of E-1-E is broken with the addition of another methylene group. The extended chain would allow for 5 unique QOOH products to be made from the δ-E-2-E ROO, which would increase possible reaction paths leading to OH-radical production.

At low temperatures, Li et al. [11] and Jacobs et al. [10] both conclude that reactions of the α-E-1-E ROO and β-E-1-E ROO radicals are the primary drivers of ignition. Cai et al. [36] confirmed that this remains true for n=2 methyl-terminated OMEs. Thus, the additional central H-atom sites would not be expected to affect the low-temperature IDT, as observed in Fig. 3. However, the first stage IDT for low temperature reactions does decrease with the oxymethylene addition (see Fig. 4). Merchant et al. [37] note the first stage IDT can be directly attributed to generation of ketohydroperoxides (KHPs) in the low temperature ignition regime. In order for KHPs to form, ROO must isomerize to QOOH, undergo a second O_2 addition to form OOQOOH, and finally undergo an internal H-atom abstraction before decomposing to form a KHP. Comparing the BDEs for E-1-E and E-2-E in Fig. 1 highlights why E-2-E has a faster first stage IDT. With the addition of another oxymethylene unit, the influence of the O-atoms on neighboring bonds is enhanced, slightly increasing the C-O bond strengths. This creates a stabilizing effect, slowing down β-scission to increase likelihood of O_2 addition to the E-2-E radicals. Paired with the previously discussed increased number of possible QOOH configurations for E-2-E, which in turn, increases the number of possible second O_2 addition sites, E-2-E is more likely to form KHPs, enhancing first stage IDT.

3.2. Effect of Lengthening the Terminating Alkyl Groups

Again referencing E-1-E as a base, the shift to P-1-P demonstrates the effect of extending the alkyl termination groups by one additional methylene per

side. In this case, the larger molecule shows similar trends to E-1-E, but at lower temperatures (up to approximately 900 K) is less reactive, and transitions towards rapid ignition at lower temperatures (around 1000 K compared to 1100 K for the E-1-E), leading to a smaller region of temperature independence than E-1-E. The rapid ignition at high temperatures speeds up to the point that above 1000 K, P-1-P reacts an order of magnitude faster than E-1-E, and slightly faster than E-2-E. Despite observable differences in the primary IDTs for E-1-E and P-1-P, the first stage ignition of both fuels have quite similar behavior.

To understand the variations in ignition behavior with the increase of the end group alkyl chain length, we consider the differences in H-abstraction kinetics between methyl ethyl ether (MEE) and methyl propyl ether (MPE). MEE and MPE are similar to E-1-E and P-1-P respectively, terminating the molecule at the first oxymethylene group. In a theoretical kinetics study of HO_2 + various ethers, Mendes et al. [38] calculated the reaction rates for abstraction at each unique H-atom site in MEE and MPE. At low temperatures (up to 500 K), 99% of all H-abstraction from the C_2 and C_3 end groups occurs on the α-carbon, and the total rates for H-abstractions at all sites on the C_2 and C_3 end groups are similar (within a factor of 1.5 with DEE abstraction occurring slightly faster). It is reasonable to expect that abstraction at the α-carbon on E-1-E and P-1-P would dominate at low temperatures, and the resultant fuel radicals would combine with O_2 to form α-ROO radicals. It is facile for the α-ROO radicals to form 6-membered ring transition states to internally abstract an H-atom. For E-1-E, a 6-centered transition state is formed to abstract the weakened δ-hydrogen, and would be expected to be the only competitive route. P-1-P has two 6-centered transition state options: internal abstraction of the δ-hydrogen similar to E-1-E, or to abstract the stronger (4.2 kcal/mol stronger) γ-hydrogen, which is unlikely to occur. Given the similar chemistry for low-temperature oxidation of E-1-E and P-1-P, it is unsurprising that first stage ignition behavior and low-temperature primary IDTs are similar.

As temperature increases, so do the deviations between the IDTs of E-1-E and P-1-P. E-1-E H-abstraction reactions increase in total rate, but continue to occur $>$97% at the α-hydrogen site. Thus, the E-1-E oxidation mechanism is unchanged with temperature, though temperature can affect subsequent branching of the ROO/QOOH/OOQOOH radical cascade to HO_2 and OH. For P-1-P, the chemistry begins to change around 1000 K, at which point only 87% of abstraction occurs at the α-hydrogen site, with the balance occurring at the β-hydrogen site. This opens a second possible OOQOOH pathway, in which the expected second O_2 addition site is still expected to be the δ-carbon. With the relocation of one peroxyl group one atom further from the oxymethylene backbone, the subsequent β-C-O bond would be expected to be weakened, promoting faster decomposition to reactive radicals. This may account for the rapid increase in P-1-P reactivity but warrants further study to confirm the role of β-hydrogen abstraction on IDTs.

3.3. Effect of Branching Terminating Alkyl Groups

The final molecule to consider is the branched OME, iP-1-iP. For this, we will compare to linear P-1-P, which shares the same chemical composition but with a different structure. In this case, iP-1-iP did not react at all in the measured time frame (400 ms after TDC) under the original test conditions of 20 bar compressed pressure, even at temperatures exceeding 1000 K. Therefore, to get reliable ignition, the pressure was increased to 30 bar, and even at these elevated pressure conditions, measurable ignition still did not occur until 900 K. However, upon reaching a point where ignition occurs, the IDT advanced rapidly, decreasing two orders of magnitude from more than 200 ms to slightly more than 3 ms in a very small temperature range, as seen in Fig. 5. No multi-stage ignition behavior occurred with this molecule at any test condition, although the ignition required temperatures outside of the multi-stage region for P-1-P.

To explain this behavior, we compare the ignition of P-1-P and iP-1-iP to previously published work by Johnson et al. [39], who studied the ignition of n-propanol and isopropanol in a shock tube at 1 atm and found that isopropanol has a longer IDT than n-propanol. However, the somewhat increased IDT for isopropanol is not enough to explain the disparate IDT behavior of P-1-P and iP-1-iP. A theoretical study on H-abstractions of n-propanol and isopropanol by OH may further clarify this behavior. Guo et al. [40] showed that for n-propanol, abstraction at the α-carbon is preferred at all temperatures above room temperature. The equivalent H-atoms in P-1-P would be either the α-hydrogens or potentially the δ-hydrogens. Both resultant radicals can readily accept addition of O_2, promoting low-temperature ignition kinetics. In contrast, Guo et al. [40] showed that for isopropanol, abstraction at the the α-carbon is only preferred below $\sim$1000 K (above $\sim$1000 K methyl group abstraction is preferred). This has significant consequences for iP-1-iP ignition. Even more so than isopropanol, the α-hydrogens in iP-1-iP are crowded. O_2 would be unlikely to add at the α-site; β-scission to less reactive products such as acetone, formaldehyde, and propene is preferred. The result would be an arresting of the ROO cascade necessary for ignition at low temperatures.

As temperature increases, the abstraction at the β-carbon sites becomes more important. At 900 K, Guo et al. [40] observed $\sim$40% of all abstraction from isopropanol occurs at the terminal methyl sites. Similarly for iP-1-iP, abstraction at the terminal methyl sites is expected to become significant at $\sim$900 K, creating β-iP-1-iP radicals which are unencumbered enough to accept the addition of O_2. These ROO radicals can then begin the ROO cascade required for ignition, and hence, this phenomenon explains the lack of observed ignition until $\sim$900 K in this work.

4. Conclusions

In this work, we consider the effect of selectively varying the molecular composition, namely, the length and structure of the terminating alkyl endgroup and the number of oxymethylene units, on non-methyl-terminated OME ignition. We find that for linear OMEs, two-stage low temperature ignition continues to occur with similar chemical pathways to methyl-terminated OMEs, and the general trends in ignition behavior are similar. Further, for the branched OME, we find that the crowding of the α-hydrogen sites inhibits low temperature reactions and that at higher temperatures the β-hydrogen sites dominate reaction, in a similar manner to analogous alcohols. The effects of the changes in structures are summarized as follows:

Oxymethylene Units: By adding an additional oxymethylene group to form E-2-E, additional QOOH structures are possible, leading to more rapid first stage low temperature IDTs and high temperature IDTs, however, the dominant pathways leading to low temperature primary ignition are unchanged.

Alkyl End Group Length: Extending the alkyl group from ethyl to propyl has little effect on reaction pathways at low temperatures, however, slower H-abstraction rates from the propyl groups slightly delay low temperature ignition. At high temperatures, additional OOQOOH structures possible via H-abstraction from β-propyl sites open up additional OH formation pathways and accelerate ignition of P-1-P.

End Group Branching: Reorienting the propyl group to an isopropyl configuration severely inhibits ignition at low to moderate temperatures due to preferential α-H-abstraction which is crowded and unlikely to bond with O_2. As a result, no low temperature ignition behavior is observed. However, at high temperatures, β-H-abstraction becomes accessible, spurring rapid ignition.

This work provides data and discussion of the ignition behaviors for several unstudied OMEs important for future chemical kinetic studies of these novel class of potentially renewable fuel blendstocks. Additional work is necessary to fully characterize the effects of the additional ROO sites for P-1-P high temperature combustion. Additionally, testing of other possible branched OMEs such as diisobutoxymethane should be performed to advance the understanding of these novel fuel molecules and determine their feasibility for engine use.

Acknowledgments

Funding for this research is provided by U.S. Department of Energy's Office of Energy Efficiency and Renewable Energy under the Bioenergy Technologies Office, Co-Optimization of Fuels and Engines Initiative award number DE-EE0008726, with additional financial support from the Colorado Energy Research Collaboratory. We thank Jon Luecke of the U.S. National Renewable Energy Laboratory for the ICN measurements. P-1-P fuel sample was provided without charge by Lambiotte & Cie in Belgium.

Supplementary Material

Table S1: Ignition Delay Times and RCM Conditions
Table S2: Access Information for Full Data Set
Fig. S1: RCM System Schematic
Fig. S2: Example of IDT Calculation Algorithm

References

[1] K. Hackbarth, P. Haltenort, U. Arnold, J. Sauer, Recent progress in the production, application and evaluation of oxymethylene ethers, Chemie Ingenieur Technik 90 (10) (2018) 1520–1528.

[2] A. Omari, B. Heuser, S. Pischinger, C. Rüdinger, Potential of long-chain oxymethylene ether and oxymethylene ether-diesel blends for ultra-low emission engines, Applied Energy 239 (2019) 1242–1249.

[3] D. Pélerin, K. Gaukel, M. Härtl, E. Jacob, G. Wachtmeister, Potentials to simplify the engine system using the alternative diesel fuels oxymethylene ether OME_1 and OME_{3-6} on a heavy-duty engine, Fuel 259 (2020) 116231.

[4] M. Härtl, P. Seidenspinner, E. Jacob, G. Wachtmeister, Oxygenate screening on a heavy-duty diesel engine and emission characteristics of highly oxygenated oxymethylene ether fuel OME_1, Fuel 153 (2015) 328–335.

[5] L. Lautenschütz, D. Oestreich, P. Seidenspinner, U. Arnold, E. Dinjus, J. Sauer, Physico-chemical properties and fuel characteristics of oxymethylene dialkyl ethers, Fuel 173 (2016) 129–137.

[6] D. L. Bartholet, M. A. Arellano-Treviño, F. L. Chan, S. Lucas, J. Zhu, P. C. St. John, T. L. Alleman, C. S. McEnally, L. D. Pfefferle, D. A. Ruddy, B. Windom, T. D. Foust, K. F. Reardon, Property predictions demonstrate that structural diversity can improve the performance of polyoxymethylene ethers as potential bio-based diesel fuels, Fuel 295 (2021) 120509.

[7] M. Kass, M. Wissink, C. Janke, R. Connatser, S. Curran, Compatibility of elastomers with polyoxymethylene dimethyl ethers and blends with diesel, Society of Automotive Engineers Technical Paper Series 1 (01) (2020).

[8] L. C. Kröger, M. Döntgen, D. Firaha, W. A. Kopp, K. Leonhard, Ab initio kinetics predictions for H-atom abstraction from diethoxymethane by hydrogen, methyl, and ethyl radicals and the subsequent unimolecular reactions, Proceedings of the Combustion Institute 37 (1) (2019) 275–282.

[9] B. Lehrheuer, F. Hoppe, K. A. Heufer, S. Jacobs, H. Minwegen, J. Klankermayer, B. Heuser, S. Pischinger, Diethoxymethane as tailor-made fuel for gasoline controlled autoignition, Proceedings of the Combustion Institute 37 (4) (2019) 4691–4698.

[10] S. Jacobs, M. Döntgen, A. B. S. Alquaity, R. Hesse, S. Kruse, J. Beeckmann, L. C. Kröger, P. Morsch, K. Leonhard, H. Pitsch, K. A. Heufer, A comprehensive experimental and kinetic modeling study of the combustion chemistry of diethoxymethane, Energy & Fuels 35 (19) (2021) 16086–16100.

[11] R. Li, J. M. Herreros, A. Tsolakis, W. Yang, Chemical kinetic modeling of diethoxymethane oxidation: A carbon–neutral fuel, Fuel 291 (2021) 120217.

[12] P. C. S. John, Y. Guan, Y. Kim, S. Kim, R. S. Paton, Prediction of organic homolytic bond dissociation enthalpies at near chemical accuracy with sub-second computational cost, Nature Communications 11 (2020) 2328.

[13] P. C. S. John, Y. Guan, Y. Kim, B. D. Etz, S. Kim, R. S. Paton, Quantum chemical calculations for over 200,000 organic radical species and 40,000 associated closed-shell molecules, Scientific Data 7 (2020) 244.

[14] P. C. St. John, Y. Guan, Y. Kim, B. D. Etz, S. Kim, R. S. Paton. BDE Estimator, available at <http://bde.ml.nrel.gov//> [online].

[15] Comparing Cetane Number Measurement Methods, Vol. ASME 2020 Internal Combustion Engine Division Fall Technical Conference of Internal Combustion Engine Division Fall Technical Conference, v001T02A009.

[16] S. McAllister, J.-Y. Chen, A. C. Fernandez-Pello, Fundamentals of combustion processes, Vol. 302, Springer, 2011.

[17] C. Zhang, J. He, Y. Li, X. Li, P. Li, Ignition delay times and chemical kinetics of diethoxymethane/O_2/Ar mixtures, Fuel 154 (2015) 346–351.

[18] M. Drexler, P. Haltenort, T. A. Zevaco, U. Arnold, J. Sauer, Synthesis of tailored oxymethylene ether (OME) fuels via transacetalization reactions, Sustainable Energy & Fuels 5 (2021) 4311–4326.

[19] L. Lautenschütz, D. Oestreich, P. Haltenort, U. Arnold, E. Dinjus, J. Sauer, Efficient synthesis of oxymethylene dimethyl ethers (OME) from dimethoxymethane and trioxane over zeolites, Fuel Processing Technology 165 (2017) 27–33.

[20] M. A. Arellano-Treviño, D. Bartholet, A. T. To, A. W. Bartling, F. G. Baddour, T. L. Alleman, E. D. Christensen, G. M. Fioroni, C. Hays, J. Luecke, J. Zhu, C. S. McEnally, L. D. Pfefferle, K. F. Reardon, T. D. Foust, D. A. Ruddy, Synthesis of butyl-exchanged polyoxymethylene ethers as renewable diesel blendstocks with improved fuel properties, ACS Sustainable Chemistry & Engineering 9 (18) (2021) 6266–6273.

[21] R. Peláez, P. Marín, S. Ordóñez, Effect of formaldehyde precursor and water inhibition in dimethoxymethane synthesis from methanol over acidic ion exchange resins: mechanism and kinetics, Biofuels, Bioproducts and Biorefining 15 (6) (2021) 1696–1708.

[22] S. P. Lucas, F. L. Chan, G. M. Fioroni, T. D. Foust, A. Gilbert, J. Luecke, C. S. McEnally, J. J. A. Serdoncillo, A. J. Zdanowicz, J. Zhu, B. Windom, Fuel properties of oxymethylene ethers with terminating groups from methyl to butyl, Energy & Fuels [In Press, DOI: 10.1021/acs.energyfuels.2c01414] (2022).

[23] J. Luecke, M. J. Rahimi, B. T. Zigler, R. W. Grout, Experimental and numerical investigation of the advanced fuel ignition delay analyzer (AFIDA) constant-volume combustion chamber as a research platform for fuel chemical kinetic mechanism validation, Fuel 265 (2020) 116929.

[24] ASTM International, ASTM D8183-18 Standard Test Method for Determination of Indicated Cetane Number (ICN) of Diesel Fuel Oils using a Constant Volume Combustion Chamber—Reference Fuels Calibration Method, 2018.

[25] ASTM International, ASTM D93-20 Standard Test Methods for Flash Point by Pensky-Martens Closed Cup Tester, 2020.

[26] J. Würmel, E. Silke, H. Curran, M. Ó Conaire, J. Simmie, The effect of diluent gases on ignition delay times in the shock tube and in the rapid compression machine, Combustion and Flame 151 (1) (2007) 289–302.

[27] C.-J. Sung, H. J. Curran, Using rapid compression machines for chemical kinetics studies, Progress in Energy and Combustion Science 44 (2014) 1–18.

[28] A. Boissiere, Effect of additives on laser ignition and compression ignition of methane and hydrocarbons in a rapid compression machine, Master's thesis, Colorado State University (2016).

[29] S. Wang, D. F. Davidson, R. K. Hanson, Chapter 3 - shock tube techniques for kinetic target data to improve reaction models, in: T. Faravelli, F. Manenti, E. Ranzi (Eds.), Mathematical Modelling of Gas-Phase Complex Reaction Systems: Pyrolysis and Combustion, Vol. 45 of Computer Aided Chemical Engineering, Elsevier, 2019, pp. 169–202.

[30] P. Zhang, I. G. Zsély, V. Samu, T. Nagy, T. Turányi, Comparison of methane combustion mechanisms using shock tube and rapid compression machine ignition delay time measurements, Energy & Fuels 35 (15) (2021) 12329–12351.

[31] M. Mehl, W. J. Pitz, C. K. Westbrook, H. J. Curran, Kinetic modeling of gasoline surrogate components and mixtures under engine conditions, Proceedings of the Combustion Institute 33 (1) (2011) 193–200.

[32] C. W. Gao, J. W. Allen, W. H. Green, R. H. West, Reaction mechanism generator: Automatic construction of chemical kinetic mechanisms, Computer Physics Communications 203 (2016) 212–225.

[33] M. Mehl, H. J. Curran, W. J. Pitz, C. K. Westbrook, Chemical kinetic modeling of component mixtures relevant to gasoline, in: 4th European Combustion Meeting, no. LLNL-CONF-410968, 2009.

[34] G. Mittal, M. Chaos, C.-J. Sung, F. L. Dryer, Dimethyl ether autoignition in a rapid compression machine: Experiments and chemical kinetic modeling, Fuel Processing Technology 89 (12) (2008) 1244–1254, dimethyl Ether Special Section.

[35] J. Ezzell, D. Wilson, C. Allen, On the influence of initial conditions and facility effects on rapid compression machine data, Fuel 245 (2019) 368–383.

[36] L. Cai, S. Jacobs, R. Langer, F. vom Lehn, K. A. Heufer, H. Pitsch, Auto-ignition of oxymethylene ethers (OME_n, n = 2–4) as promising synthetic e-fuels from renewable electricity: shock tube experiments and automatic mechanism generation, Fuel 264 (2020) 116711.

[37] S. S. Merchant, C. F. Goldsmith, A. G. Vandeputte, M. P. Burke, S. J. Klippenstein, W. H. Green, Understanding low-temperature first-stage ignition delay: Propane, Combustion and Flame 162 (10) (2015) 3658–3673.

[38] J. Mendes, C.-W. Zhou, H. J. Curran, Rate constant calculations of H-atom abstraction reactions from ethers by HO_2 radicals, The Journal of Physical Chemistry A 118 (8) (2014) 1300–1308, pMID: 24483837.

[39] M. V. Johnson, S. S. Goldsborough, Z. Serinyel, P. O'Toole, E. Larkin, G. O'Malley, H. J. Curran, A shock tube study of n- and iso-propanol ignition, Energy & Fuels 23 (12) (2009) 5886–5898.

[40] X. Guo, R. M. Zhang, L. G. Gao, X. Zhang, X. Xu, Computational kinetics of the hydrogen abstraction reactions of n-propanol and iso-propanol by OH radical, Phys. Chem. Chem. Phys. 21 (2019) 24458–24468.